Proceeding Paper

Fatigue Strength Determination of AISI 316L Steel and Welded Specimens Using Energy Methods †

Danilo D'Andrea *[ID], **Giacomo Risitano** [ID], **Pasqualino Corigliano** [ID] and **Davide D'Andrea** [ID]

Dipartimento di Ingegneria, Università di Messina, Contrada di Dio, Sant'Agata, 98166 Messina, Italy;
giacomo.risitano@unime.it (G.R.); pasqualino.corigliano@unime.it (P.C.);
davide.dandrea@studenti.unime.it (D.D.)
*   Correspondence: dandread@unime.it
†   Presented at the 53rd Conference of the Italian Scientific Society of Mechanical Engineering Design (AIAS 2024), Naples, Italy, 4–7 September 2024.

Abstract: AISI 316 is a stainless steel known for its exceptional corrosion resistance and excellent mechanical properties. It is used in the chemical and pharmaceutical industries, food processing equipment, and medical devices. This alloy's wide range of applications underscores its importance in industries requiring materials that can withstand extreme conditions while maintaining structural integrity and performance. Additionally, the excellent weldability and formability of AISI 316 allow for versatile design and production processes, ensuring durable and reliable performance in marine environments. This work aims to examine the behavior of AISI 316L and its welded joints under high-cycle fatigue loadings using infrared thermography (IR). Two kinds of experimental tests are performed on specimens with the same geometry: static tests and stepwise succession tests. The results of the static tests are in accordance with the stepwise succession test results in predicting the fatigue properties.

Keywords: AISI 316L; thermography; fatigue; welding; energy methods; shipbuilding

1. Introduction

AISI 316L stainless steel is one of the most important kinds of austenitic stainless steel, and it is known for its excellent mechanical properties and high corrosion resistance [1]. It is widely used in many industrial industries, such as marine [2,3], biomedical [4,5], or aerospace [6].

Furthermore, thanks to its excellent weldability, AISI 316L is used to fabricate equipment subjected to welding processes [7], such as pipes [8], automotive exhaust gas systems, chemical industrial equipment, and naval parts [9,10]. Corigliano et al. recently reviewed the types of loadings and materials commonly faced in the maritime industry [11]. A ship, during its lifetime, faces standard sea-state conditions and can face storms with large wave amplitudes; these produce high stress values with localized plasticity that induce low-cycle fatigue loadings, which should be considered a major failure mode associated with ultimate or accidental limit states [11,12], as well as compression loadings that could accelerate the collapse due to instability [13]. Fajri et al. [14] analyzed five structural elements in the midship section of a vessel using the FEM (Finite Element Method), as this area was found to be the most prone to fatigue failure. Four different materials were used: high-strength low-alloy (HSLA) SAE 950X steel, medium carbon steel, and stainless steels of types 316L and 304. The medium carbon steel exhibited higher fatigue resistance but showed negligible resistance to corrosion, which could lead to crack formation. Although the other

steels had a shorter fatigue life, they demonstrated good corrosion resistance. In 2021, Akbar et al. [15] studied the strength of plated-hull structures as a function of hydrostatic and hydrodynamic forces using a 600 TEU container ship as a case study. The deformation values for the stainless steel investigated were lower than the permissible limits, confirming their suitability for design use. Moreover, the challenges become more intricate when evaluating welded joints. Nonetheless, the inherently complex welding process, which often leads to induced defects, residual stresses, and microstructural alterations, results in lower fatigue resistance in welded connection regions compared to steel [16].

The mentioned studies confirm the need to continue investigating the material's fatigue properties. On the other hand, evaluating mechanical properties, especially the fatigue behavior of common engineering materials, requires extensive testing campaigns involving large quantities of specimens and time.

However, applying energy methods, such as infrared thermography [17], for assessing the fatigue limit significantly shortens the required testing time while ensuring reliable results [18,19]. Thermography is a widely used technique for the mechanical characterization of materials and is recognized by the scientific community [20–22]. The development of the Risitano Thermographic Method (RTM) allows for the evaluation of the material's fatigue limit and the S-N curve, exploiting the heating of the materials when subjected to cyclic loads beyond the fatigue limit [23]. In the last ten years, the Static Thermographic Method (STM) has been proposed to evaluate the first damage initiation within the material by monitoring the superficial temperature evolution during a static tensile test. A "first damage stress" could be identified when the temperature decrease deviates from the linear thermoelastic trend. The STM has been applied to several materials and compared with conventional constant amplitude fatigue tests and the RTM, showing good agreement. This work aims to compare traditional AISI 316L specimens and welded specimens using energy methods. To obtain the mechanical behavior of AISI 316L, static tensile tests and stepwise tests were performed, monitoring the energy release of the material using the Static Thermographic Method (STM) and Risitano Thermographic Method (RTM). The results show that welding negatively influences the fatigue behavior of the material.

2. Theoretical Background

In 1968, Risitano used infrared thermography to assess material fatigue [17]. Later, in 2000, La Rosa and Risitano developed the Thermographic Method to determine the fatigue life of materials [24]. When a material is subjected to cyclic loading beyond its fatigue limit, three distinct temperature evolution phases can be observed (Figure 1a): an initial increase (I), a stabilization phase (II), and a subsequent rise in temperature (III). The higher the applied stress, the greater the stabilization temperature in Phase II; however, the area under the temperature vs. cycle number curve remains constant and corresponds to an energy parameter Φ. By applying different stress levels progressively [23] (Figure 1b), it is possible to determine the stabilization temperature for each stress condition. The fatigue limit is identified at the intersection of the temperature vs. stress curve with the stress axis [24].

Among different rapid fatigue assessment methods, the Static Thermographic Method has shown the possibility of rapidly obtaining the first damage initiation within the material. The STM is related to the variation in the temperature trend that exhibits three different phases during a static tensile test (Figure 2). The first phase (I) is characterized by an initial approximately linear decrease due to the thermoelastic effect described by Lord Kelvin's law. In the second phase (II), the temperature deviates from the first linear trend until a minimum temperature value is reached. In the last phase (III), the temperature

increases rapidly until the material fails (III). Under uniaxial stress state and in adiabatic test conditions, Lord Kelvin's law can be expressed as Equation (1):

$$\Delta T_s = -K_m T \sigma_1 = -\frac{\alpha}{\rho c} T \sigma_1 \tag{1}$$

where the temperature variation ΔT_s depends on Km, the thermoelastic constant of the material; T, the actual temperature of the specimen; and Iσ, the first invariant of the stress tensor.
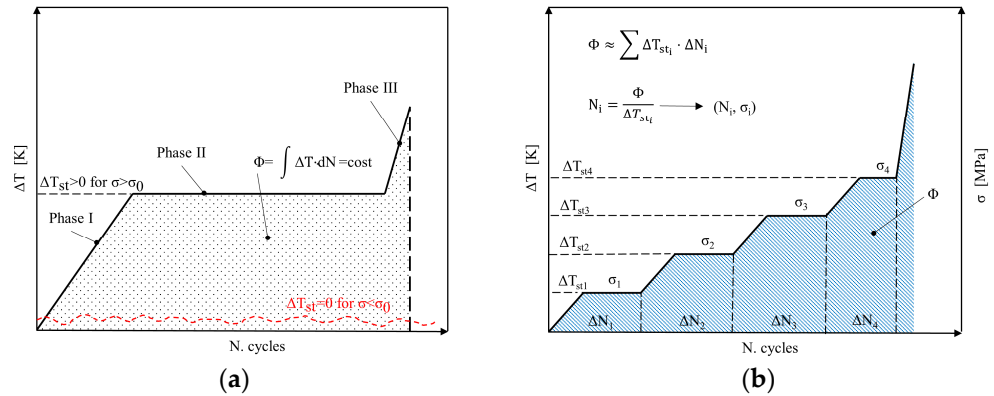

Figure 1. Temperature evolution during (**a**) constant amplitude and (**b**) stepwise fatigue tests [25].
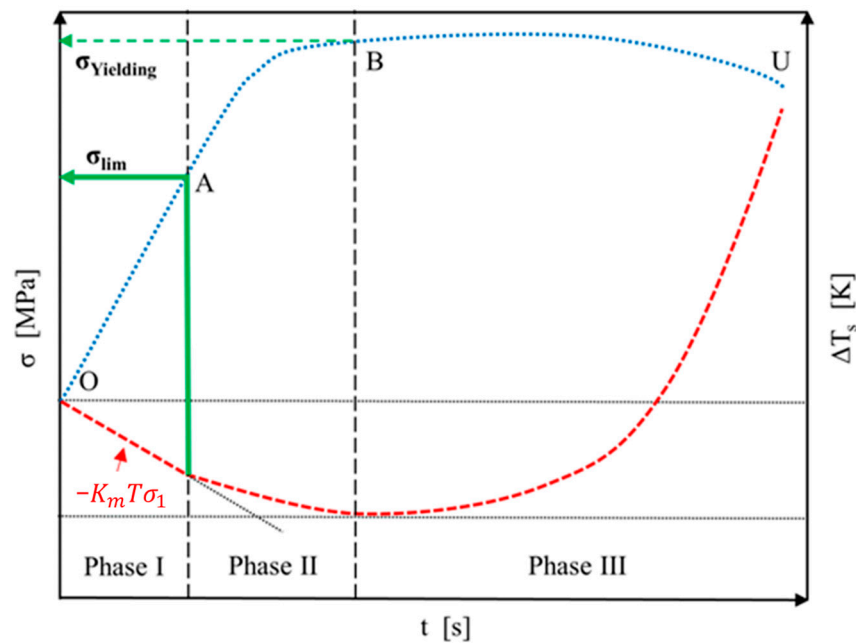
Figure 2. Temperature trend during a static tensile test [26].

The transition point between Phase I and Phase II may be related to a macroscopic stress level, the limit stress able to be produced within the material microcracks. If that stress level is applied cyclically to the specimen, it will result in fatigue failure.

3. Materials and Methods

To evaluate the fatigue behavior of traditional and welding AISI 316L, static and stepwise tests were performed on two sets of specimens, the "as-received" and the "welded" one (Figure 3). The first set of samples was obtained by laser cutting from a 3 mm thick plate, while the "welded" samples were made via the V-shaped welding of two plates. A full penetration welding without filler material was executed. The welding bead was

subsequently flattened. The set of "welded" specimens was also made by laser cutting. Static tensile tests were performed under stress control with a stress rate equal to 6 MPa/s, using a servo-hydraulic loading machine MTS 810 with a maximum load capacity of 250 kN. The stress rate must be adopted to ensure adiabatic conditions during the tensile tests, i.e., the specimen must not have the time to exchange heat with the surrounding environment. During the tests, the specimen surface temperature was monitored using an infrared camera, FLIR A40, to record the temperature evolution every second. For the post-processing of the temperature signal, a rlowess filter was used, with a data span of 5%, to exclude outliers and enhance the linear trend.
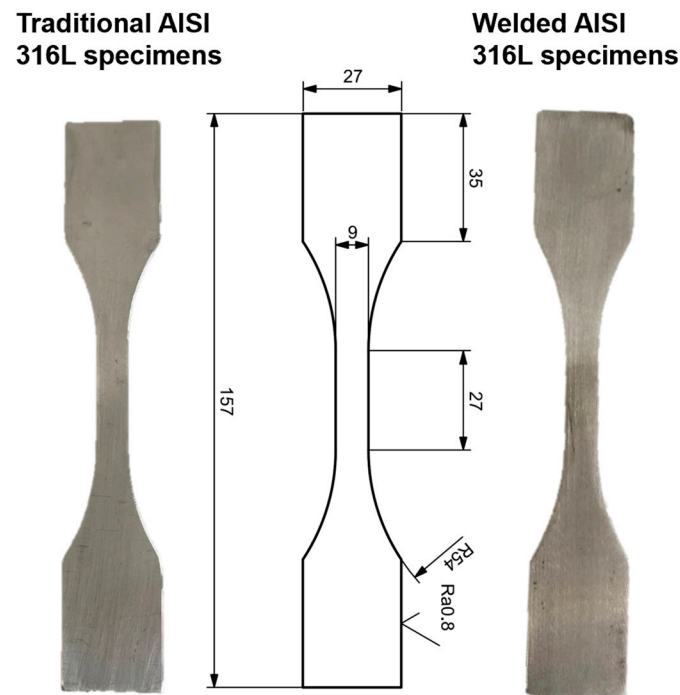

Figure 3. AISI 316L specimens (3 mm thickness).

Stepwise fatigue tests were performed on five specimens, adopting a positive stress ratio (R = 0.1), with test frequencies of 10 Hz and a number of cycles per block ΔN of 20,000 cycles. During all the tests, the temperature trend was monitored using a FLIR A40 IR thermal imaging camera (320 × 240 pixel, thermal sensitivity of 0.08 °C to 30 °C).

4. Results and Discussion

4.1. Static Tensile Test

To assess the "fatigue limit" stress using the Static Thermographic Method, several preliminary tests were conducted at 3 MPa/s, 4 MPa/s, and 6 MPa/s, with the latter providing the best reliable adiabatic conditions to better determine the thermal phenomenon. During the tests, an IR thermal imaging camera was used to evaluate the temperature signal variation on the specimen surface as the difference between the initial and instantaneous temperature values. The temperature signal was filtered using a rlowess filter with a data span of 5%. The stress curve was plotted against the temperature variation and time to correlate the stress level with the energy release of the material.

The Figure 4 shows the application of the STM on the "as-received" AISI 316L specimen. It is possible to underline how the first part of the temperature signal has a linear trend (dashed line) due to the thermoelastic effect of the material. Then, in the second part (the dot-and-dash line), the temperature deviates from linearity until it reaches a minimum, and finally, it experiences a very high further increment until failure. To evaluate the limit

stress, σ_{lim}, it is possible to draw two linear regression lines for the linear and non-linear parts, respectively, and determine their equations. By solving the system of equations, it is possible to determine the intersection point of the two lines corresponding to the value of σ_{lim} on the stress–strain curve. For AISI 316L "as-received", the value of the limit stress determined equals $\sigma_{lim} = 204 \pm 8$ MPa.
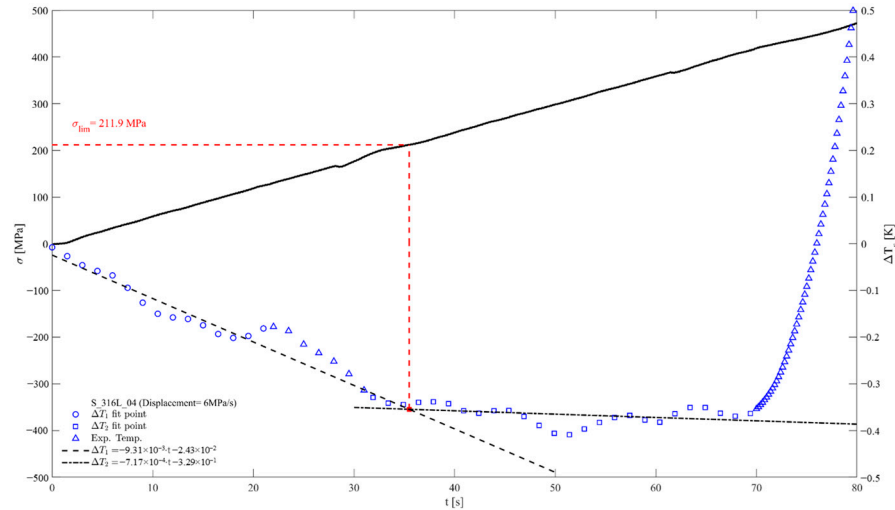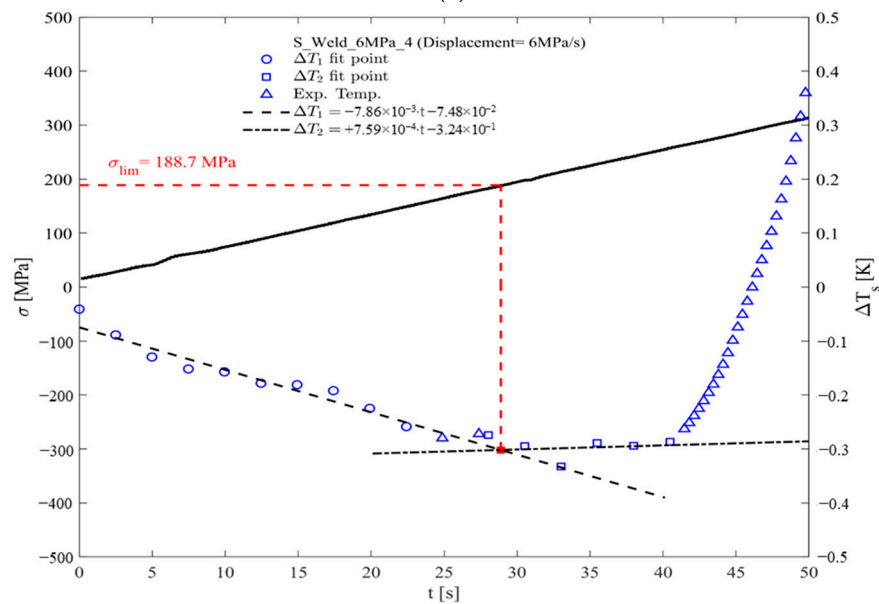
Figure 4. Static Thermography Method (STM) applied on AISI 316L specimens: (**a**) "as-received"; (**b**) "welded".

The same procedure was applied to the AISI 316L welded samples (Figure 4b); in this case, monitoring the thermal signal made it possible to clearly distinguish the two different phases, and the average value obtained was $\sigma_{lim} = 191 \pm 20$ MPa.

Table 1 reports the mechanical properties, i.e., the ultimate tensile strength and the limit stress, obtained using the static tensile tests performed on the "as-received" and "welded" specimens. The as-received samples exhibit a higher ultimate tensile strength compared to the welded samples, with the welded specimens showing greater variability. This difference can be attributed to the welding process, which often induces defects in the weld zone and introduces residual stresses. Similarly, the limit stress is higher for the as-received material than for the welded specimens. This behavior, as noted in several

experimental studies on AISI stainless steels and other materials, can be explained by microstructural defects introduced during the welding process [27–30].

Table 1. Mechanical properties for AISI 316L.

Specimen Type	No. Specimen	σ_U [MPa]	σ_{lim} [MPa]	σU_{ave} [MPa]	$\sigma_{lim\,ave}$ [MPa]
"as-received"	1	675	201		
	2	687	212	667 ± 20	204 ± 8
	3	638	200		
"welded"	1	617	189		
	2	611	211	580 ± 67	191 ± 20
	3	513	172		

4.2. Fatigue Test

In order to confirm the STM results, several stepwise tests were performed on as-received AISI 316L samples using stress ratios of R = 0.1. As described in Section 2, to determine the fatigue limit stress, different stabilization temperatures for each stress level and the energy parameter Φ of the sample were evaluated (Figure 5). Table 2 shows the stress levels and the corresponding number of cycles for the test shown in Figure 5. As described by the Risitano Thermographic Method, for stress levels below the assumed fatigue limit of the material, the temperature increments are negligible. However, as the applied stress level increases, the dissipated energy, or rather the surface temperature of the specimen, reaches a higher level.

Figure 5. Temperature evolution during a stepwise fatigue test of "as-received" AISI 316L at R = 0.1.

Table 2. Stepwise test parameters.

σ_{max} [MPa]	200	220	240	260	280	300
N_{cycle}	20,000	20,000	20,000	20,000	20,000	20,000

For example, it is possible to plot different stabilization temperatures vs. applied stress levels (Figure 6). It is possible to intersect a straight line with the points related to the stress levels above the presumed fatigue limit, just as it is possible to intersect a straight line with the points related to the stress levels below the fatigue limit. The intersection of the two intersecting lines corresponds to the stress levels at which fatigue damage begins. Therefore, it can be related to the fatigue limit of the material.
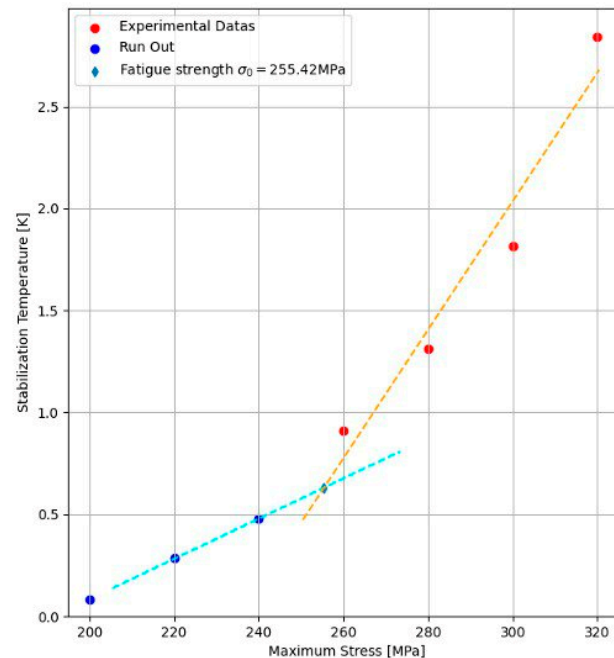

Figure 6. Stabilization temperature vs. applied stress level for "as-received" AISI 316L at stress ratio R 0.1.

For "as-received" AISI 316L tested using the stepwise fatigue test, with stress ratio R = 0.1, a value of fatigue limit $\sigma_{lim,RTM}$ = 255 MPa was found. The fatigue limit value obtained using the RTM at R = 0.1 is approximately 20% higher than that obtained using the STM. However, considering the scientific literature, an $\sigma_{lim,RTM}$ value at least 40% higher than that obtained using the STM was expected. This can be justified by the different geometry and type of specimen processing compared to the scientific works of Santonocito et al. [25] and Crisafulli et al. [26]. In fact, in these cited works, the specimens were obtained by turning and had an hourglass geometry with a useful section area of 78.5 mm^2. In the present work, the specimens have a flat dog-bone geometry with a useful section area of 27 mm^2 and were obtained using a rolling process. The results obtained are influenced by the size effect [31] and the microstructure and different manufacturing processes of flat specimens compared to hourglass ones. Further studies and in-depth analyses will be carried out to correlate the size effect with the mechanical behavior of the AISI316L.

5. Conclusions

In this work, the mechanical properties, particularly the fatigue life, of AISI 316L were evaluated. Two sets of samples were tested, one "as-received" and the other called "welded", characterized by welded specimens. To determine the mechanical behavior of the investigated specimens, energetic methods were used, particularly the Static Thermographic Method (STM) and the Risitano Thermographic Method (RTM).

The results show that the STM and RTM allow for the quick and accurate identification of the fatigue limit value. The fatigue limit value obtained using the RTM at R = 0.1 was approximately 20% higher than that obtained with the STM. To confirm the results obtained

using energy methods, constant amplitude fatigue testing campaigns will be conducted. The "welded" specimens, evaluated with STM, as expected, show a worsening of the mechanical properties compared to the "as-received" specimens. However, further test campaigns are planned, especially on the "welded" specimens to accurately and precisely evaluate the value of the fatigue limit. Further stepwise tests and traditional fatigue tests will be performed, as well as microstructural analyses to correlate the mechanical behavior to the microstructure of AISI 316L.

Author Contributions: Conceptualization, D.D. (Danilo D'Andrea) and P.C.; methodology, D.D. (Danilo D'Andrea), P.C. and G.R.; validation, D.D. (Danilo D'Andrea) and G.R.; investigation, D.D. (Danilo D'Andrea) and D.D. (Davide D'Andrea); data curation, D.D. (Danilo D'Andrea) and D.D. (Davide D'Andrea); writing—original draft preparation, D.D. (Danilo D'Andrea) and D.D. (Davide D'Andrea); writing—review and editing, D.D. (Davide D'Andrea); visualization, D.D. (Davide D'Andrea); supervision, G.R.; funding acquisition, P.C. All authors have read and agreed to the published version of the manuscript.

Institutional Review Board Statement: Not applicable.

Informed Consent Statement: Not applicable.

Data Availability Statement: Data are contained within the article.

Conflicts of Interest: The authors declare no conflicts of interest.

References

1. D'Andrea, D. Additive Manufacturing of AISI 316L Stainless Steel: A Review. *Metals* **2023**, *13*, 1370. [CrossRef]
2. Ren, Z.; Ernst, F. Stress–Corrosion Cracking of Aisi 316L Stainless Steel in Seawater Environments: Effect of Surface Machining. *Metals* **2020**, *10*, 1324. [CrossRef]
3. Daille, L.K.; Aguirre, J.; Fischer, D.; Galarce, C.; Armijo, F.; Pizarro, G.E.; Walczak, M.; De la Iglesia, R.; Vargas, I.T. Effect of Tidal Cycles on Bacterial Biofilm Formation and Biocorrosion of Stainless Steel AISI 316L. *J. Mar. Sci. Eng.* **2020**, *8*, 124. [CrossRef]
4. Taqriban, R.B.; Ismail, R.; Jamari, J.; Bayuseno, A.P. Finite Element Analysis of Artificial Hip Joint Implant Made from Stainless Steel 316L. *Bali Med. J.* **2021**, *10*, 448–452. [CrossRef]
5. Fellah, M.; Labaïz, M.; Assala, O.; Dekhil, L.; Zerniz, N.; Iost, A. Tribological Behavior of Biomaterial for Total Hip Prosthesis. *Matériaux Tech.* **2014**, *102*, 601. [CrossRef]
6. Pradeep, P.I.; Kumar, V.A.; Sriranganath, A.; Singh, S.K.; Sahu, A.; Kumar, T.S.; Narayanan, P.R.; Arumugam, M.; Mohan, M. Characterization and Qualification of LPBF Additively Manufactured AISI-316L Stainless Steel Brackets for Aerospace Application. *Trans. Indian Natl. Acad. Eng.* **2020**, *5*, 603–616. [CrossRef]
7. Lothongkum, G.; Viyanit, E.; Bhandhubanyong, P. Study on the Effects of Pulsed TIG Welding Parameters on Delta-Ferrite Content, Shape Factor and Bead Quality in Orbital Welding of AISI 316L Stainless Steel Plate. *J. Mater. Process Technol.* **2001**, *110*, 233–238. [CrossRef]
8. Jiang, X.; Wang, W.; Xu, C.; Li, J.; Lu, J. Effect of Process Parameters on Welding Residual Stress of 316L Stainless Steel Pipe. *Materials* **2024**, *17*, 2201. [CrossRef]
9. Kaya, Y.; Kahraman, N. An Investigation into the Explosive Welding/Cladding of Grade A Ship Steel/AISI 316L Austenitic Stainless Steel. *Mater. Des.* **2013**, *52*, 367–372. [CrossRef]
10. Vinoth, V.; Sathiyamurthy, S.; Prabhakaran, J.; Sanjeevi Prakash, K.; Mohamed Suhail, H.; Sundaravignesh, S. Tensile, Impact and Non-Destructive Analysis of 316L Stainless Steel for Marine Applications. *J. Manuf. Eng.* **2023**, *18*, 130–135. [CrossRef]
11. Corigliano, P.; Frisone, F.; Chianese, C.; Altosole, M.; Piscopo, V.; Scamardella, A. Fatigue Overview of Ship Structures under Induced Wave Loads. *J. Mar. Sci. Eng.* **2024**, *12*, 1608. [CrossRef]
12. Gledić, I.; Parunov, J.; Prebeg, P.; Ćorak, M. Low-Cycle Fatigue of Ship Hull Damaged in Collision. *Eng. Fail. Anal.* **2019**, *96*, 436–454. [CrossRef]
13. Corigliano, P. On the Compression Instability during Static and Low-Cycle Fatigue Loadings of AA 5083 Welded Joints: Full-Field and Numerical Analyses. *J. Mar. Sci. Eng.* **2022**, *10*, 212. [CrossRef]

14. Fajri, A.; Prabowo, A.R.; Muhayat, N. Assessment of Ship Structure under Fatigue Loading: FE Benchmarking and Extended Performance Analysis. *Curved Layer. Struct.* **2022**, *9*, 163–186. [CrossRef]

15. Akbar, M.S.; Prabowo, A.R.; Tjahjana, D.D.D.P.; Tuswan, T. Analysis of Plated-Hull Structure Strength against Hydrostatic and Hydrodynamic Loads: A Case Study of 600 TEU Container Ships. *J. Mech. Behav. Mater.* **2021**, *30*, 237–248. [CrossRef]

16. Barsoum, Z. *Guidelines for Fatigue and Static Analysis of Welded and Un-Welded Steel Structures*; TRITA-SCI-RAP; KTH Royal Institute of Technology: Stockholm, Sweden, 2020; ISBN 978-91-7873-478-8.

17. Curti, G.; La Rosa, G.; Orlando, M.; Risitano, A. Analisi Tramite Infrarosso Termico Della Temperatura Limite in Prove Di Fatica. In Proceedings of the XIV Convegno Nazionale AIAS, Catania, Italy, 23–27 September 1986; pp. 211–220.

18. D'Andrea, D.; Risitano, G.; Guglielmino, E.; Piperopoulos, E.; Santonocito, D. Correlation between Mechanical Behaviour and Microstructural Features of AISI 316L Produced by SLM. *Procedia Struct. Integr.* **2022**, *41*, 199–207. [CrossRef]

19. Corigliano, P.; Crupi, V.; Epasto, G.; Guglielmino, E.; Risitano, G. Fatigue Assessment by Thermal Analysis during Tensile Tests on Steel. *Procedia Eng.* **2015**, *109*, 210–218. [CrossRef]

20. Wagner, D.; Ranc, N.; Bathias, C.; Paris, P.C. Fatigue Crack Initiation Detection by an Infrared Thermography Method. *Fatigue Fract. Eng. Mater. Struct.* **2010**, *33*, 12–21. [CrossRef]

21. Sapieta, M.; Dekýš, V.; Kaco, M.; Pástor, M.; Sapietová, A.; Drvárová, B. Investigation of the Mechanical Properties of Spur Involute Gearing by Infrared Thermography. *Appl. Sci.* **2023**, *13*, 5988. [CrossRef]

22. Seelan, P.J.; Dulieu-Barton, J.M.; Pierron, F. Microstructural Assessment of 316L Stainless Steel Using Infrared Thermography Based Measurement of Energy Dissipation Arising from Cyclic Loading. *Mech. Mater.* **2020**, *148*, 103455. [CrossRef]

23. Fargione, G.; Geraci, A.; La Rosa, G.; Risitano, A. Rapid Determination of the Fatigue Curve by the Thermographic Method. *Int. J. Fatigue* **2002**, *24*, 11–19. [CrossRef]

24. La Rosa, G.; Risitano, A. Thermographic Methodology for Rapid Determination of the Fatigue Limit of Materials and Mechanical Components. *Int. J. Fatigue* **2000**, *22*, 65–73. [CrossRef]

25. Santonocito, D.; Fintová, S.; Di Cocco, V.; Iacoviello, F.; Risitano, G.; D'Andrea, D. Comparison on Mechanical Behaviour and Microstructural Features Between Traditional and AM AISI 316L. *Fatigue Fract. Eng. Mater. Struct.* **2023**, *46*, 379–395. [CrossRef]

26. Crisafulli, D.; Fintová, S.; Santonocito, D.; D'Andrea, D. Microstructural Characterization and Mechanical Behaviour of Laser Powder Bed Fusion Stainless Steel 316L. *Theor. Appl. Fract. Mech.* **2024**, *131*, 104343. [CrossRef]

27. Gustavo, F.; Pereira, L.; Lourenço, J.M.; Maribondo Do Nascimento, R.; Castro, A. Fracture Behavior and Fatigue Performance of Inconel 625. *Mater. Res.* **2018**, *21*, 20171089. [CrossRef]

28. Schroeder, R.M.; Müller, I.L. Fatigue and Corrosion Fatigue Behavior of 13Cr and Duplex Stainless Steel and a Welded Nickel Alloy Employed in Oil and Gas Production. *Mater. Corros.* **2009**, *60*, 365–371. [CrossRef]

29. Heide Lambertsen, S.; Damkilde, L.; Schmidt Kristensen, A.; Refstrup Pedersen, R. Estimation of Fatigue Life of Laser Welded AISI304 Stainless Steel T-Joint Based on Experiments and Recommendations in Design Codes. *World J. Mech.* **2013**, *3*, 178–183. [CrossRef]

30. Fomin, F.; Horstmann, M.; Huber, N.; Kashaev, N. Probabilistic Fatigue-Life Assessment Model for Laser-Welded Ti-6Al-4V Butt Joints in the High-Cycle Fatigue Regime. *Int. J. Fatigue* **2018**, *116*, 22–35. [CrossRef]

31. Tomaszewski, T. Statistical size effect in fatigue properties for mini-specimens. *Materials* **2020**, *13*, 2384. [CrossRef]